Contribution from the Departments of Chemistry, Waseda University, Shinjuku-ku, Tokyo 169, Japan, and Toho University, Funabashi, Chiba 274, Japan

Synthesis, Crystal Structure, and ^{13}C NMR Spectra of α-Pyrrolidonato-Bridged Head-to-Head $[Pt^{III}_2(NH_3)_4(C_4H_6NO)_2(NO_2)(NO_3)](NO_3)_2\cdot H_2O$ and Electrochemical Study on Conversion of the Binuclear Platinum(III) Complex into a Tetranuclear Platinum(III) Complex

Takeya Abe,[1a] Hiroshi Moriyama,[1b] and Kazuko Matsumoto*,[1a]

Received January 3, 1991

The α-pyrrolidonate-bridged binuclear Pt(III) complex $[Pt^{III}_2(NH_3)_4(C_4H_6NO)_2(NO_2)(NO_3)](NO_3)_2\cdot H_2O$ was prepared by oxidation of $[Pt^{II}_2Pt^{III}_2(NH_3)_8(C_4H_6NO)_4](NO_3)_6\cdot 2H_2O$ with HNO_3. The crystal structure, ^{13}C and ^{195}Pt NMR and UV-vis spectra, and the electrochemical properties are reported. The crystal is monoclinic, $P2_1/c$, with the cell dimensions a = 10.019 (2) Å, b = 25.196 (6) Å, c = 9.714 (4) Å, β = 112.39 (2)°, Z = 4, and V = 2267 (1) Å^3. The two Pt(III) atoms are bridged by two α-pyrrolidonate ligands in a head-to-head manner. Each Pt(III) atom is also coordinated by two NH_3 groups in cis position. One of the Pt atoms is axially coordinated by NO_2^- and the other is by NO_3^-. Cyclic voltammogram of the compound in 0.05 M H_2SO_4 shows an irreversible redox wave at E_{pc} = 0.12 V and E_{pa} = 0.70 V vs SCE; however, the wave gradually changes to E_{pc} = 0.48 V and E_{pa} = 0.55 V after repetitive cyclic scans. This change corresponds to the electrochemical reduction of the compound to $[Pt^{II}_2(NH_3)_4(C_4H_6NO)_2]^{2+}$, which is then electrochemically oxidized not to the original compound but to $[Pt^{III}_4(NH_3)_8(C_4H_6NO)_4]^{8+}$. Therefore, on repeated scans, the original binuclear Pt(III) compound is gradually converted to a tetranuclear Pt(III) compound.

Introduction

Among a number of amidate-bridged binuclear[2-5] or tetranuclear[6-9] platinum complexes related to so-called "platinum blues",[10-13] α-pyrrolidonate-bridged tetranuclear platinum tan, $[Pt^{II}_2Pt^{III}_2(NH_3)_8(C_4H_6NO)_4]^{6+}$[7,8] (**1a**), is one of the most intensively studied complexes in the sense that it is the only example that is isolated as the $[Pt^{II}_2Pt^{III}_2]$ tan oxidation state, compared with all other complexes of the $[Pt^{III}Pt^{II}_3]$ blue oxidation state with different amidate bridging ligands. Novel multistep reversible redox behavior has been clarified for **1a** as the first example in this class of compounds. Reduction of **1a** by OH^- affords a binuclear Pt(II) complex, $[Pt^{II}_2(NH_3)_4(C_4H_6NO)_2]^{2+}$,[14] whereas oxidation of **1a** by $S_2O_8^{2-}$ gives the tetranuclear Pt(III) complex $[Pt^{III}_4(NH_3)_8(C_4H_6NO)_4]^{8+}$ (**2a**).[15] Although compound **2a** has not yet been structurally characterized by X-ray analysis, solid-state ESR study of **2a** and its reduced form suggests that **2a** is basically similar in structure to **1a** and $[Pt^{II}_3Pt^{III}(NH_3)_8(C_4H_6NO)_4]^{5+}$ (**3a**).[15] All of these cationic complexes exhibit in cyclic voltammetry, regardless of their platinum oxidation states, a single redox wave at 0.53 V vs. SCE, which corresponds to the following redox reaction from the highest to the lowest oxidation states of the complex: $[Pt^{III}_4(NH_3)_8(C_4H_6NO)_4]^{8+}$ (**2a**) + 4e $\rightleftarrows$ $2[Pt^{II}_2(NH_3)_4(C_4H_6NO)_2]^{2+}$. However, the single wave consists actually of several very close-lying redox waves involving the intermediate oxidation states **3a** and **1a**, besides $[Pt^{II}_2(NH_3)_4(C_4H_6NO)_2]^{2+}$ (**4a**) and **2a**.[16] In the present study, a binuclear Pt(III) complex with α-pyrrolidonate bridging ligands, $[Pt^{III}_2(NH_3)_4(C_4H_6NO)_2(NO_2)(NO_3)](NO_3)_2\cdot H_2O$ (**5**), was synthesized by oxidation of **1a** with HNO_3. Although the binuclear complex **5** is analogous to the previously reported α-pyridonate-bridged binuclear Pt(III) complex,[17,18] the present study demonstrates for the first time that both binuclear and tetranuclear Pt(III) complexes exist as oxidized forms of **1a**, their formation conditions depending on the oxidizing agent used and the nature of the ligands coexisting in the solution. Novel electrochemical interconversion of the two oxidized forms is also reported, and these facts would contribute to a better understanding of the complicated solution behavior and the redox chemistry of this class of complexes. The synthesis and the crystal structure of **5** have been briefly reported previously.[19] Details of the structure, the spectroscopic properties, and the electrochemical properties are presented here.

Table I. Crystallographic Data for $[Pt^{III}_2(NH_3)_4(\alpha\text{-pyrrolidonato})_2(NO_2)(NO_3)](NO_3)_2\cdot H_2O$

chem formula: $Pt_2C_8H_{26}N_{10}O_{14}$	Z = 4
fw = 876.57	T = 23 °C
cryst syst: monoclinic	λ = 0.716 068 Å
space group: $P2_1/C$ (No. 14)	ρ_{obsd} = 2.61 g cm^{-3}
a = 10.019 (2) Å	ρ_{calcd} = 2.57 g cm^{-3}
b = 25.196 (6) Å	μ = 125.4 cm^{-1}
c = 9.714 (4) Å	transm factors: 1.000-0.839
β = 112.39 (2)°	R = 0.045
V = 2267 (1) Å^3	R_w = 0.047 ($w = 1/\sigma^2(F)$)

Experimental Section

Preparation of the Complex. The binuclear Pt(III) complex **5** was prepared by suspending 0.1 g of **1**[7,8] in 10 mL of 3 M HNO_3. While the solution was left at room temperature for a week, it turned from dark red to yellow, and yellow prism-shaped crystals appeared (yield 60%). Anal. Calcd for $Pt_2C_8H_{26}N_{10}O_{14}$: C, 10.96; H, 2.99; N, 15.98. Found: C, 11.23; H, 2.75; N, 16.01.

The mixed sulfate, perchlorate salt of the tetranuclear Pt(III) complex **2a**, $[Pt^{III}_4(NH_3)_8(C_4H_6NO)_4](SO_4)_2(ClO_4)_4\cdot 6H_2O$ (**2**), was prepared according to the previously reported method.[15]

α-Pyrrolidonate-Coordinated Binuclear Pt(III) Complex with Axially Coordinated *N*-Methylimidazole (Me-Im). $[Pt^{III}_2(NH_3)_4(C_4H_6NO)_2(Me\text{-}Im)(SO_4)](PF_6)_2\cdot 0.5H_2O$ (**6**) was prepared by adding 2 equiv of *N*-methylimidazole to a saturated 1.8 M H_2SO_4 solution of **2**, which was prepared from **1** and $Na_2S_2O_8$ as described previously.[15] Addition of a

(1) (a) Waseda University. (b) Toho University.
(2) Hollis, L. S.; Lippard, S. J. *J. Am. Chem. Soc.* **1983**, *105*, 3494.
(3) Lippert, B.; Neugebauer, D.; Schubert, U. *Inorg. Chim. Acta* **1980**, *46*, L11.
(4) Schollhorn, H.; Thewalt, U.; Lippert, B. *Inorg. Chim. Acta* **1984**, *93*, 19.
(5) Lippert, B.; Neugebauer, D.; Raudaschl, G. *Inorg. Chim. Acta* **1983**, *78*, 161.
(6) Laurent, M. P.; Tewksbury, J. C.; Krogh-Jespersen, M.-B.; Patterson, H. *Inorg. Chem.* **1980**, *19*, 1656.
(7) Matsumoto, K.; Fuwa, K. *J. Am. Chem. Soc.* **1982**, *104*, 897.
(8) Matsumoto, K.; Takahashi, H.; Fuwa, K. *Inorg. Chem.* **1983**, *22*, 4086.
(9) O'Halloran, T. V.; Mascharak, P. K.; Williams, I. D.; Roberts, M. M.; Lippard, S. J. *Inorg. Chem.* **1987**, *26*, 1261.
(10) Barton, J. K.; Rabinowitz, H. N.; Szalda, D. J.; Lippard, S. J. *J. Am. Chem. Soc.* **1977**, *99*, 2827.
(11) Barton, J. K.; Szalda, D. J.; Rabinowitz, H. N.; Waszczak, J. V.; Lippard, S. J. *J. Am. Chem. Soc.* **1978**, *101*, 1434.
(12) Barton, J. K.; Caravana, C.; Lippard, S. J. *J. Am. Chem. Soc.* **1979**, *101*, 7269.
(13) Hollis, L. S.; Lippard, S. J. *J. Am. Chem. Soc.* **1981**, *103*, 1230.
(14) Matsumoto, K.; Miyamae, H.; Moriyama, H. *Inorg. Chem.* **1989**, *28*, 2959.
(15) Matsumoto, K.; Watanabe, T. *J. Am. Chem. Soc.* **1986**, *108*, 1308.
(16) Matsumoto, K.; Matoba, N. *Inorg. Chim. Acta* **1988**, *142*, 59.
(17) Hollis, L. S.; Lippard, S. J. *Inorg. Chem.* **1983**, *22*, 2605.
(18) O'Halloran, T. V.; Roberts, M. M.; Lippard, S. J. *Inorg. Chem.* **1986**, *25*, 957.
(19) Abe, T.; Moriyama, H.; Matsumoto, K. *Chem. Lett.* **1989**, 1857.

0020-1669/91/1330-4198$02.50/0

Scheme I

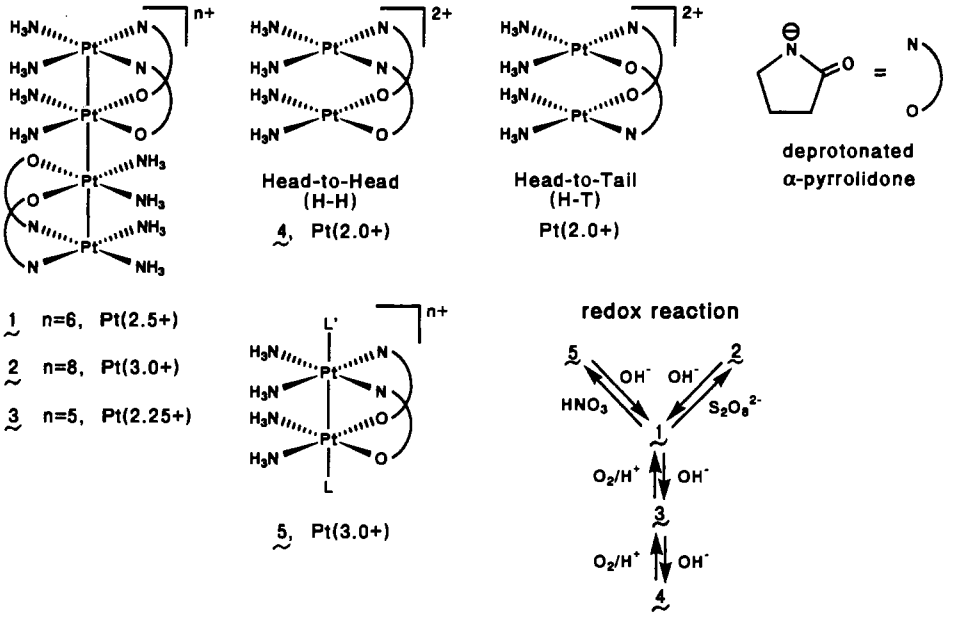

slight excess of $NaPF_6$ and cooling of the solution at 5 °C gave a yellow precipitate of **6**. Anal. Calcd for $Pt_2C_{12}H_{31}N_8O_{6.5}$: C, 13.08; H, 3.21; N, 10.17. Found: C, 13.49; H, 3.32; N, 10.05.

Physical Measurements. The electrochemical measurements were performed on a Fuso 315A potentiostat with a platinum-disk working electrode and a platinum wire as a counter electrode. All of the measurements were performed with a three-electrode system by using SCE as a reference electrode.

UV–vis spectra were obtained on a Shimadzu UV-260 spectrophotometer.

^{13}C CP/MAS NMR measurement was performed on a Bruker MSL400 instrument at 100.6 MHz, whereas ^{13}C solution NMR data were measured on a Bruker AC200P instrument at 50.3 MHz. The ^{13}C and ^{195}Pt measurements of **2** and **6** were carried out at 0 °C, since the aqueous solutions of these complexes are not stable at room temperature. The ^{195}Pt NMR spectra were acquired on a JEOL FX90A spectrometer. Chemical shift data for ^{13}C NMR spectroscopy are reported relative to TMS, which is set in a sealed coaxial capillary tube in a 5-mm sample tube, whereas a saturated solution of K_2PtCl_6 in D_2O was used as an external reference for ^{195}Pt chemical shift data.

Collection and Reduction of X-ray Data. X-ray diffraction measurement was performed on a Rigaku AFC-5R instrument with graphite-monochromated Mo Kα radiation. A crystal coated with epoxide resin was used for measurement, since the crystal is unstable toward X-ray and humidity. Unit cell parameters were obtained from a least-squares fit of 24 reflections in the range $15° < 2\theta < 28°$. The details of the data collection are given in Table I and in supplementary Table S1. The density of the crystal was measured by a flotation method with CH_3-Cl–CH_3Br.

Solution and Refinement of the Structure. The coordinates of the two platinum atoms were determined from a Patterson map, and a series of block-diagonal least-squares refinements followed by Fourier synthesis revealed all the remaining atoms except hydrogen atoms. The structure was finally refined with anisotropic temperature factors for all the atoms to the final discrepancy index of $R = 0.045$ and $R_w = 0.047$, where $R = \sum||F_o| - |F_c||/\sum|F_o|$ and $R_w = [\sum w_i(|F_o| - |F_c|)^2/\sum w_i|F_o|^2]^{1/2}$ ($w_i = 1/\sigma^2(F_o)$). Atomic scattering factors and anomalous dispersion corrections were referred to ref 20. All of the calculations were performed with the program system UNICS-III[21] and ORTEP.[22] Absorption correction was made by following the method of North et al.[23] None of the hydrogen atoms was located in the final difference map, and therefore they were not included in the calculation.

The final positional and thermal parameters are listed in Table II. The anisotropic temperature factors with their standard deviations (Table S2) and the observed and calculated structure factors (Table S3) are available as supplementary materials.

Table II. Atomic Parameters and Isotropic Thermal Parameters[a]

atom	x	y	z	B_{eq}, Å^2
Pt1	70384 (6)	9993 (2)	31184 (6)	162 (2)
Pt2	68790 (6)	14328 (2)	55296 (6)	169 (2)
NH1	5610 (13)	384 (5)	2811 (14)	24 (4)
NH2	8737 (14)	474 (6)	4116 (14)	30 (4)
NH3	5395 (14)	939 (5)	5835 (14)	27 (4)
NH4	8532 (15)	1016 (5)	7035 (14)	30 (4)
N1	5396 (12)	1494 (5)	2079 (12)	21 (4)
O1	5244 (11)	1866 (4)	4175 (11)	28 (4)
C11	4808 (15)	1810 (6)	2750 (16)	21 (4)
C12	3516 (19)	2111 (7)	1686 (18)	33 (6)
C13	3555 (19)	1976 (8)	153 (18)	37 (6)
C14	4660 (20)	1499 (8)	421 (17)	44 (6)
N2	8489 (12)	1585 (5)	3351 (12)	20 (4)
O2	8356 (11)	1963 (4)	5481 (12)	30 (4)
C21	8853 (16)	1923 (6)	4412 (16)	23 (5)
C22	10033 (20)	2307 (7)	4425 (20)	40 (7)
C23	10432 (18)	2079 (7)	3151 (18)	33 (6)
C24	9265 (20)	1654 (8)	2331 (19)	43 (7)
ND	6776 (16)	1883 (6)	7304 (14)	33 (5)
OD1	7072 (22)	1666 (6)	8494 (15)	77 (8)
OD2	6566 (19)	2358 (6)	7087 (18)	70 (7)
NA	12208 (16)	1084 (7)	6553 (17)	47 (6)
OA1	13222 (17)	1412 (7)	6807 (20)	80 (8)
OA2	12505 (30)	636 (7)	6378 (28)	130 (14)
OA3	11076 (18)	1198 (11)	6490 (26)	139 (12)
NB	7720 (14)	−370 (5)	6682 (14)	29 (4)
OB1	6735 (14)	−65 (5)	5845 (13)	40 (4)
OB2	8984 (14)	−229 (6)	7077 (17)	58 (6)
OB3	7307 (14)	−789 (5)	7051 (15)	46 (5)
WAT	10732 (29)	913 (13)	9858 (22)	171 (14)
NC(1)	7290 (31)	324 (12)	277 (30)	36 (10)
OC1(1)	7010 (33)	381 (13)	−1155 (30)	64 (12)
OC2(1)	7519 (25)	717 (9)	1042 (23)	32 (8)
OC3(1)	7644 (40)	−31 (12)	1118 (32)	67 (14)
NC(2)	6755 (30)	441 (11)	−44 (26)	32 (9)
OC1(2)	7048 (30)	328 (12)	−1100 (27)	51 (10)
OC2(2)	7037 (23)	821 (8)	733 (23)	30 (7)
OC3(2)	5792 (41)	163 (16)	87 (39)	94 (17)

[a] Positional parameters are multiplied by 10^4, those for Pt by 10^5. B_{eq} values are multiplied by 10^1, those for Pt by 10^2.

Results

Structure of the Complex Cation. The structure of **5** with the atomic numbering scheme is shown in Figure 1. Pt1 is octahedrally coordinated by two ammine ligands in the cis position, two

(20) *International Tables for X-ray Crystallography*; Kynoch Press: Birmingham, England, 1974; Vol. IV, pp 99, 149.
(21) Sakurai, T.; Kobayashi, K. *Rikagaku Kenkyusho Hokoku* **1979**, *55*, 69.
(22) Johnson, C. K. *Report ORNL-3794* (revised); Oak Ridge National Laboratory: Oak Ridge, TN, 1976.
(23) North, A. T. C.; Philips, D. C.; Mathews, F. S. *Acta Crystallogr.* **1968**, *A24*, 351.

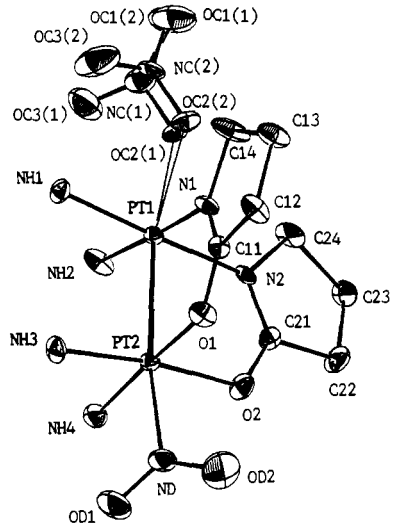

Figure 1. Molecular structure of H-H $[Pt^{III}_2(NH_3)_4(C_4H_6NO)_2(NO_2)(NO_3)]^{2+}$. The thermal ellipsoids are drawn at the 50% probability level.

deprotonated α-pyrrolidonate nitrogen atoms, and a nitrate oxygen atom and is metal–metal bonded to Pt2 with a Pt1–Pt2 separation of 2.644 (1) Å. Pt2 is coordinated by two ammine ligands in the cis position, two α-pyrrolidonate oxygen atoms, and a nitrite nitrogen atom. The two α-pyrrolidonate ligands bridge the two Pt(III) atoms in a head-to-head (H-H) manner (Scheme I).[24,25] The axially coordinated nitrate ligand is situated in two different orientations each with 50% probability as shown in Figure 1. The statistical probability was determined by least-squares refinement. The crystal packing in the unit cell is depicted in the supplementary material (Figure S1).

^{13}C CP/MAS and ^{13}C and ^{195}Pt Solution NMR. The ^{13}C CP/MAS NMR spectrum of **5** is presented in Figure 2a. The assignment of each peak is based on our previous NMR study of the α-pyrrolidonate-bridged Pt(II) dimer complex $[Pt^{II}_2(NH_3)_4(C_4H_6NO)_2]^{2+}$.[14] The ^{13}C solution NMR spectrum in 3.6 M D_2SO_4 is shown in Figure 2b. Both solid and solution spectra are basically identical and consistent with the crystal structure shown in Figure 1. The ^{13}C NMR spectrum of **2** measured at 0 °C in 3.6 M D_2SO_4 shows peaks at 19.90 (C1), 31.31 (C2), 51.83 (C3), and 190.03 (C4) ppm with $^3J_{C-Pt}$ for C2 of 38.60 Hz. The ^{13}C spectrum of **6** is shown in Figure 3. The ^{195}Pt NMR spectrum of **2** in 3.6 M D_2SO_4 measured at 0 °C shows peaks at −316 and −843 ppm, whereas that of **6** in 3.6 M D_2SO_4 exhibits peaks at 205 and −845 ppm.

Discussion

Chemical Properties of the Complexes. The yellow complex **5** is diamagnetic and is fairly stable in air; however, if it is left in air for a prolonged period of time (approximately a month), it becomes gradually reddish even in the solid state. The reddish powder is ESR silent, which is contrasted to the fact that the α-pyrrolidonate-bridged tetranuclear Pt(III) complex **2** is also diamagnetic but is very easily reduced by humidity (the originally yellow powder becomes reddish or sometimes blue) to show the ESR signal that is typical of the tetranuclear $[Pt^{II}_3Pt^{III}]$ blue oxidation state.[15] Compound **5** can be recrystallized from a concentrated aqueous solution; however, a dilute solution of **5** very easily becomes reddish, from which only **1** is obtained on concentration of the solution. Complex **6** is diamagnetic and is also an α-pyrrolidonate-bridged binuclear Pt(III) complex axially coordinated by Me-Im and sulfate ion. As described in the following, the complex is H–H and is axially coordinated presumably by Me-Im at the N_2O_2-coordinated Pt atom and by a sulfate ion at the N_4-coordinated Pt atom. Complex **6** is more stable in the solid state compared to **2**, but is less stable compared to **5**, and the originally yellow aqueous solution of **6** easily becomes reddish at room temperature. The solution further gradually turns pale blue after sufficient time and gives the ESR signal of the $[Pt^{II}_3Pt^{III}]$ blue oxidation state. These facts demonstrate that the stability of α-pyrrolidonate-bridged binuclear Pt(III) complexes is considerably affected by the axial ligands.

Table III. List of Distances (Å)

Coordination Sphere			
Pt1–Pt2	2.644 (1)	Pt1–OC2(2)	2.36 (2)
Pt1–N1	2.00 (1)	Pt2–O1	1.99 (1)
Pt1–N2	2.02 (1)	Pt2–O2	2.01 (1)
Pt1–NH1	2.05 (1)	Pt2–NH3	2.05 (1)
Pt1–NH2	2.08 (1)	Pt2–NH4	2.03 (1)
Pt1–OC2(2)	2.36 (3)	Pt2–ND	2.10 (2)
Ligand Geometry			
N1–C11	1.30 (2)	C23–C24	1.56 (2)
O1–C11	1.29 (2)	C24–N2	1.49 (3)
C11–C12	1.52 (2)	NC(1)–OC1(1)	1.32 (4)
C12–C13	1.54 (3)	NC(1)–OC2(1)	1.21 (4)
C13–C14	1.59 (3)	NC(1)–OC3(1)	1.17 (4)
C14–N1	1.49 (2)	NC(2)–OC1(2)	1.20 (4)
N2–C21	1.28 (2)	NC(2)–OC2(2)	1.19 (3)
O2–C21	1.32 (2)	NC(2)–OC3(2)	1.24 (5)
C21–C22	1.52 (3)	ND–OD1	1.21 (2)
C22–C23	1.55 (3)	ND–OD2	1.22 (2)
Anion Geometry			
NA–OA1	1.26 (2)	NB–OB1	1.27 (2)
NA–OA2	1.19 (3)	NB–OB2	1.23 (2)
NA–OA3	1.15 (3)	NB–OB3	1.24 (2)

Description of the Structure. The structure of the complex **5** is shown in Figure 1. The two α-pyrrolidonate ligands bridge the two Pt(III) atoms in a H–H manner, and the structure is analogous to that of the previously reported α-pyridonate-bridged Pt(III) dimer complex, H–H $[Pt_2(NH_3)_4(\alpha\text{-pyridonato})_2(NO_2)(NO_3)](NO_3)_2\cdot 0.5H_2O$[18] in the sense that the both complexes are the H–H isomer and a nitrite anion is coordinated to the Pt atom which is coordinated by amidate oxygen atoms (N_2O_2 coordination), whereas a nitrate anion is coordinated to the Pt atom which is coordinated by amidate nitrogen atoms (N_4 coordination). This selective nitrite coordination to a N_2O_2-coordinated Pt atom seems to result from the fact that the axial coordination site of the N_2O_2-coordinated Pt atom is sterically less crowded compared to that of the N_4-coordinated Pt atom, because the ring carbon atoms of α-pyrrolidonate are projected outward toward the axial coordination site of the N_4-coordinated Pt atom. Therefore, the nitrogen atom of a nitrite ion can more easily reach the N_2O_2-coordinated Pt atom than the N_4-coordinated Pt atom. This preferential coordination to the N_2O_2-coordinated Pt atom is less pronounced for the oxygen atom of a nitrate ion, since a nitrate oxygen atom is sterically and geometrically more favorable for any coordination site compared to a nitrite nitrogen atom. The preferential coordination of NO_3^- to the N_2O_2-coordinated Pt atom is also explained by the harder nature of an oxygen atom of NO_3^- compared with a nitrogen atom of NO_2^-. The harder N_2O_2-coordinated Pt atom would prefer the coordination of the harder ligand NO_3^-. Selected bond distances are listed in Table III, and bond angles are summarized in Table IV.

In Figure 4 the two orientations of the nitrate ligands in **5** are shown as they are observed along the Pt–Pt bond from the axial coordination position. The nitrate plane in Figure 4a is oriented as if the nitrate plane bisects the N1–Pt1–N2 angle. The oxygen atom of the nitrate ion OC3(1) is hydrogen-bonded to two ammine ligands: OC3(1)···NH1 = 3.24 (4) Å and OC3(1)···NH2 = 2.98 (3) Å. The oxygen atom OC2(1) is also hydrogen-bonded to two ammine ligands: OC2(1)···NH1 = 3.13 (3) Å and OC2(1)···NH2 = 2.83 (2) Å. The other nitrate plane shown in Figure 4b is oriented in such a way so that the nitrate plane is almost overlapped on the plane NH1–Pt–α-pyrrolidonate (plane 2). The

(24) O'Halloran, T. V.; Lippard, S. J. *J. Am. Chem. Soc.* **1983**, *105*, 3341.
(25) O'Halloran, T. V.; Lippard, S. J. *Inorg. Chem.* **1989**, *28*, 1289.
(26) Lippert, B.; Schollhorn, H.; Thewalt, U. *J. Am. Chem. Soc.* **1986**, *108*, 525.

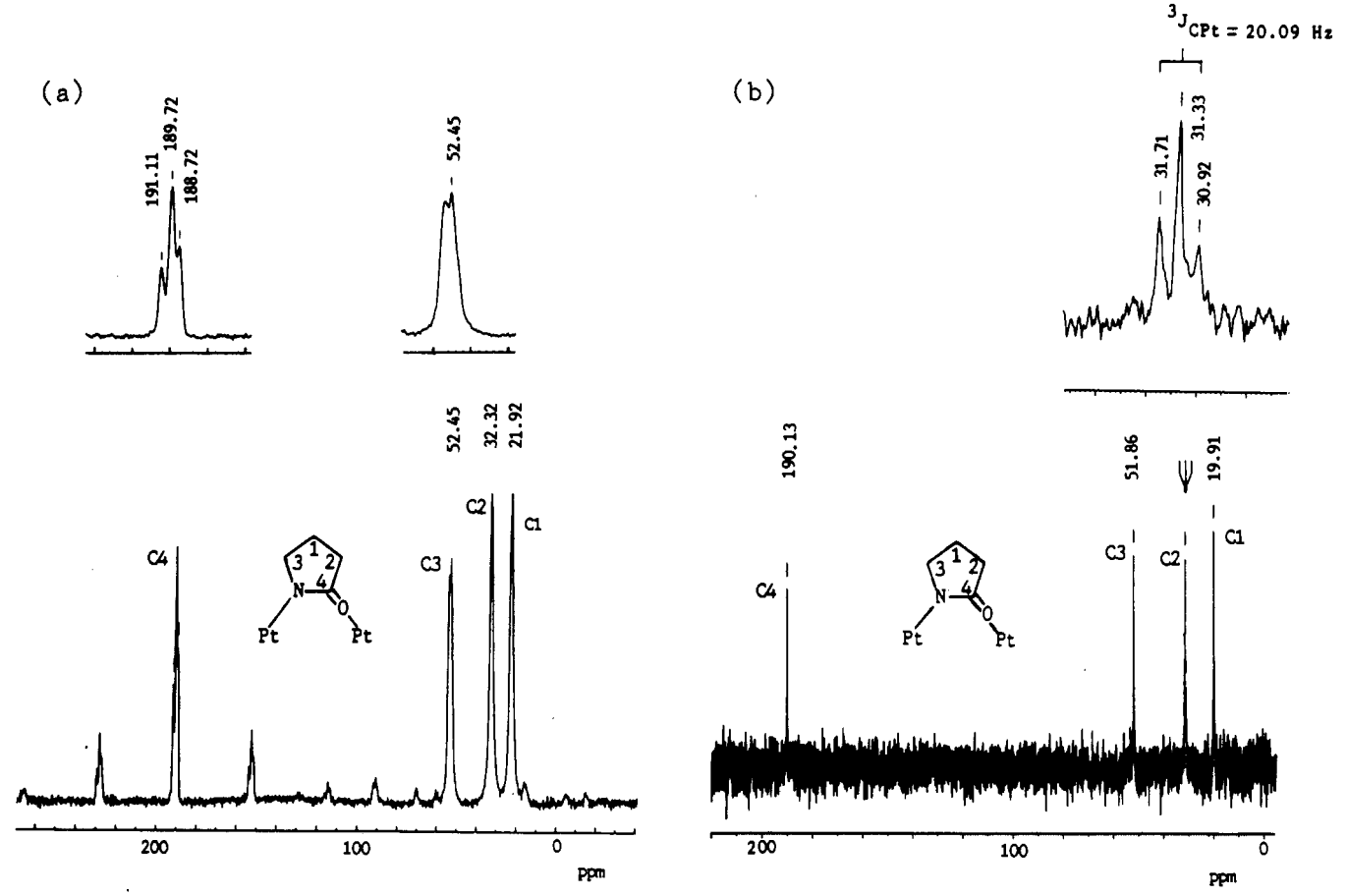

Figure 2. (a) ^{13}C CP/MAS NMR spectrum of **5**. Smaller peaks at both sides of the C4 peak are side bands. (b) ^{13}C NMR spectrum of **5** in 3.6 M D_2SO_4.

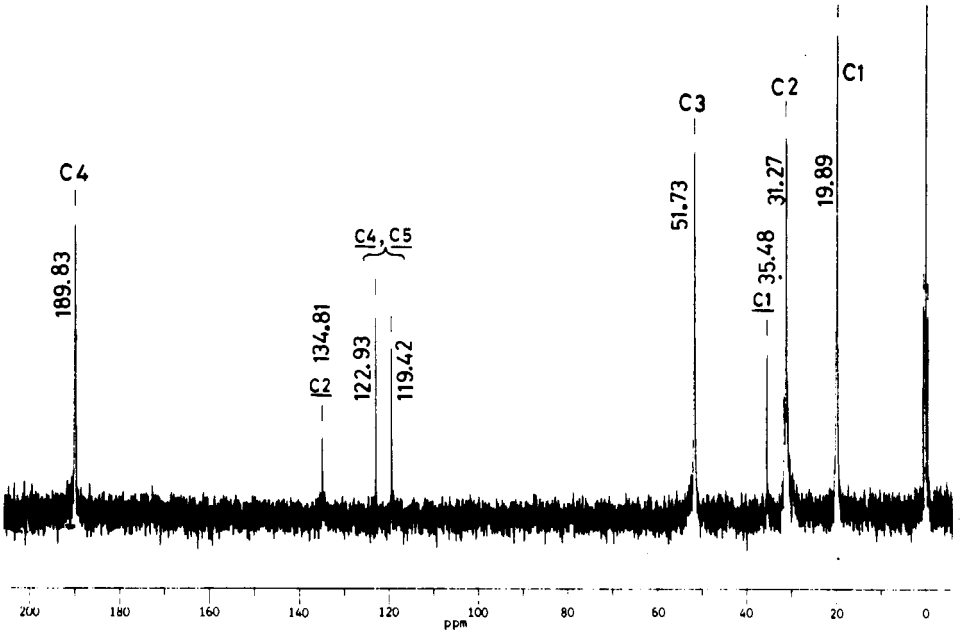

Figure 3. ^{13}C NMR spectrum of **6** in 3.6 M D_2SO_4. $^3J_{C-Pt}$ for C2 is 37.23 Hz. C1, C2, C4, and C5 are carbon atoms of Me-Im.

nitrate oxygen OC3(2) is hydrogen-bonded to NH1 (2.78 (4) Å), and OC2(2) is hydrogen-bonded to NH1 (3.09 (3) Å) and to NH2 (3.19 (2) Å). All other possible hydrogen bondings in the crystal lattice are summarized in Table S4 in the supplementary material.

The Pt–N distances (Table III) for both ammine ligands and α-pyrrolidonate ligands are within 2.02–2.08 Å, which is a normal range found in the related Pt(II) and Pt(III) complexes.[2-5,16-18] The Pt–O(α-pyrrolidonate) bond distances in **5** are also in the usual range (1.99–2.07 Å)[16-18] for Pt(III) dimer complexes and compare favorably with the same bond distances, 2.03 (4)–2.12 (3) Å, in the related tetranuclear α-pyrrolidonate tan $[Pt^{II}_2Pt^{III}_2(NH_3)_8(C_4H_6NO)_4](NO_3)_6\cdot 2H_2O$.[8]

Geometrical comparisons of analogous amidate-bridged binuclear Pt(III) complexes are given in Table V. The tilt angle (τ) between the adjacent equatorial coordination planes in **5** is 19.6°, which is almost comparable to those of the *N*-methyluracilate-bridged Pt(III) dimer and the ammine-coordinated α-pyridonate Pt(III) dimer, but is significantly smaller than that of the α-py-

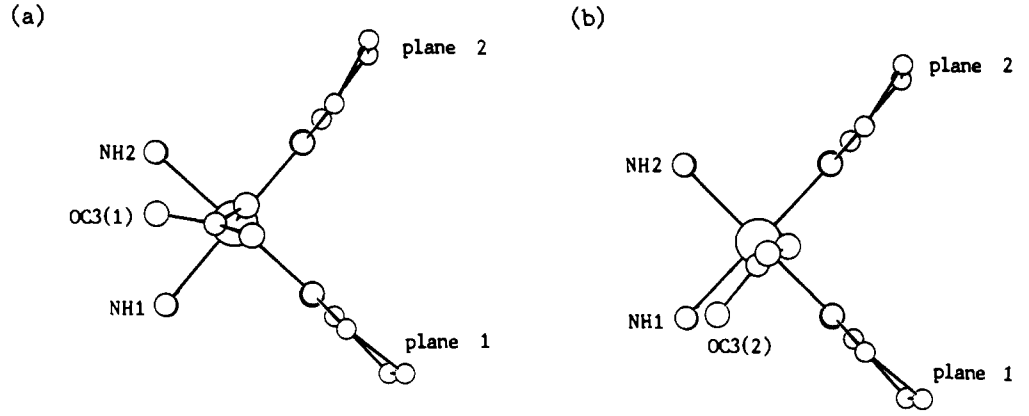

Figure 4. Two nitrate orientations as viewed along the Pt1–Pt2 vector.

Table IV. List of Angles (deg)

	Coordination Sphere		
OC2(1)-PT1-PT2	169.9 (6)	NH1-PT1-N1	177.8 (5)
OC2(1)-PT1-N1	98.8 (6)	NH1-PT1-N2	89.2 (5)
OC2(1)-PT1-N2	86.8 (7)	N1-PT1-N2	91.1 (5)
OC2(1)-PT1-NH1	90.3 (7)	ND-PT2-PT1	171.7 (4)
OC2(1)-PT1-NH2	79.0 (6)	ND-PT2-O1	87.7 (5)
OC2(2)-PT1-PT2	166.1 (5)	ND-PT2-O2	85.8 (6)
OC2(2)-PT1-N1	86.0 (6)	ND-PT2-NH3	86.8 (6)
OC2(2)-PT1-N2	88.8 (6)	ND-PT2-NH4	88.3 (5)
OC2(2)-PT1-NH1	88.5 (7)	NH3-PT2-O1	88.2 (5)
OC2(2)-PT1-NH2	91.8 (6)	NH3-PT2-O2	172.5 (5)
OC2(1)-PT1-OC2	13.0 (7)	NH3-PT2-NH4	91.1 (5)
NH1-PT1-N1	90.2 (5)	NH4-PT2-O1	176.0 (5)
NH1-PT1-N2	176.9 (6)	NH4-PT2-O2	87.4 (5)
NH1-PT1-NH2	89.4 (5)	O1-PT1-O2	92.7 (4)
	Ligand Geometry		
PT1-N1-C11	125 (1)	N2-C21-O2	128 (1)
PT1-N1-C14	121 (1)	N2-C21-C22	114 (2)
C11-N1-C14	114 (1)	O2-C21-C22	118 (1)
PT2-O1-C11	120 (1)	C21-C22-C23	101 (1)
N1-C11-O1	125 (1)	C22-C23-C24	107 (2)
N1-C11-C12	113 (1)	C23-C24-N1	103 (1)
O1-C11-C12	122 (1)	OC1(1)-NC(1)-OC2(1)	118 (3)
C11-C12-C13	103 (1)	OC2(1)-NC(1)-OC3(1)	105 (3)
C12-C13-C14	106 (1)	OC3(1)-NC(1)-OC1(1)	135 (3)
C13-C14-N1	102 (1)	OC1(2)-NC(2)-OC2(2)	131 (3)
PT1-N2-C12	123 (1)	OC2(2)-NC(2)-OC3(2)	114 (3)
PT1-N2-C24	123 (1)	OC3(2)-NC(2)-OC1(2)	114 (3)
C21-N2-C24	113 (1)	OD1-ND-OD2	125 (2)
PT2-O2-C21	118 (1)		
	Anion Geometry		
OA1-NA-OA2	115 (2)	OB1-NB-OB2	119 (1)
OA2-NA-OA3	123 (2)	OB2-NB-OB3	116 (1)
OA3-NA-OA1	122 (2)	OB3-NB-OB1	125 (1)

ridonate-bridged en-coordinated Pt(III) dimer. The torsion angle ω, or twist about the Pt–Pt vector, is 0.0°, which is also comparable to that of the *N*-methyluracilate-bridged Pt(III) dimer, but is significantly smaller than those in α-pyridonate-bridged complexes. This significant difference in the torsion angle between α-pyrrolidonate-bridged and α-pyridonate-bridged Pt complexes has been observed also in Pt(II) dimer complexes[14] and the tetranuclear tan complex.[8] It has previously been described that the tilt angle τ increases with the Pt–Pt distance in a straightforward manner;[18] however, the tendency is not clear in Table V. Presumably the range of the Pt–Pt distances in Table V is too small and such a relationship between τ and the Pt–Pt distance would be obscured by the slight deviations caused by other factors. The present Pt(III) dimer complex has the largest Pt–Pt distance (2.644 (1) Å) ever reported for amidate-bridged Pt(III) dimer complexes and also has the smallest torsion angle ω (0.0°). It is rather unusual that ω is 0.0°, but it signifies that in **5** the ammine ligands coordinated to the two Pt(III) atoms minimize the nonbonded repulsion between them not by twisting the two Pt coordination planes but by increasing the Pt–Pt distance. The Pt–Pt distance in **5** is the largest Pt(III)–Pt(III) distance so far reported for this class of complexes.

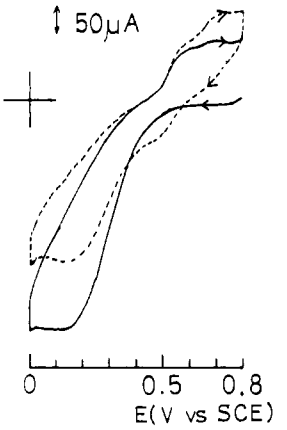

Figure 5. Cyclic voltammogram of **5** (1.0 mM in 0.05 M H_2SO_4, sweep rate 100 mV/s): (—) first cycle; (···) stationary cycle after several repetitive sweeps.

It is noteworthy that the axial Pt–O(nitrate) distances in Table V are significantly different from each other among the complexes

Table V. Comparison of Geometric Properties of Head-to-Head Pt(III) Dimers[c]

compound	distance, Å		dihedral angle,[a] deg		ref
	Pt–Pt	Pt–L(axial)	τ	ω	
$[Pt_2(NH_3)_4(C_4H_6NO)_2(NO_2)(NO_3)](NO_3)_2 \cdot H_2O$	2.644 (1)	2.36 (3) (NO_3^-) 2.36 (2) (NO_3^-) 2.10 (2) (NO_2^-)	19.6	0.0	*b*
$[Pt_2(NH_3)_4(C_5H_4NO)_2(H_2O)(NO_3)](NO_3)_3 \cdot 2H_2O$	2.5401 (5)	2.193 (7) (NO_3^-) 2.122 (6) (H_2O)	20.0	23.2	17
$[Pt_2(en)_2(C_5H_4NO)_2(NO_2)(NO_3)](NO_3)_2 \cdot 0.5H_2O$	2.6382 (6)	2.307 (11) (NO_3^-) 2.109 (11) (NO_2^-)	30.7	36.2	18
$[Pt_2(NH_3)_4(C_5H_5N_2O_2)_2(NO_2)](NO_3)_3 \cdot H_2O$	2.607 (1)	2.06 (2) (NO_2^-)	19.0	3.6	26

[a] τ is the tilt angle between adjacent Pt coordination planes in the ligand bridging unit, and ω is the torsion angle about the Pt–Pt vector. [b] This work. [c] C_5H_6NO is α-pyrrolidonate, C_5H_4NO is α-pyridonate, and $C_5H_5N_2O_2$ is *N*-methyluracilate.

in the table. It is evident that the distance is larger as the Pt–Pt distance increases. The longer axial distance and the longer Pt(III)–Pt(III) separation presumably reflect that the platinum atom is virtually in a slightly lower oxidation state than Pt(III), compared to those in other compounds shown in Table V. This virtual Pt oxidation state would be considerably affected by the degree of the donating nature of the deprotonated amidate ligand, and therefore, the Pt–Pt distance and the Pt–O(nitrate) distance depend on the nature of the amidate ligand. The bond lengths and angles within the α-pyrrolidonate ligands are similar to those found in the related structure determinations.[8,14,27]

A clear example of the structural trans influence mediated by a metal–metal bond can be seen in the Pt–N(nitrite), 2.10 (2) Å, and Pt–O(nitrate) distances, 2.36 (3) and 2.36 (2) Å, in **5**. The former value is significantly shorter than the axial Pt–N(nitrite) distances in H–T $[Pt^{III}_2(NH_3)_4(\alpha\text{-pyridonato})_2(NO_2)_2]^{2+}$,[28,29] 2.170 (10) and 2.168 (11) Å, while the latter distance is significantly longer than the Pt–O(nitrate) distances in H–T $[Pt^{III}_2(NH_3)_4(\alpha\text{-pyridonato})_2(NO_3)_2]^{2+}$,[28,29] 2.170 (10) and 2.165 (10) Å, and in H–H $[Pt^{III}_2(NH_3)_4(\alpha\text{-pyridonato})_2(H_2O)(NO_3)]^{3+}$, 2.193 (7) Å.[17-30] These differences are due to the different abilities of the various axial groups to weaken the trans axial ligand to Pt bond across the metal–metal bond axis and were reported previously for the analogous α-pyridonate-bridged Pt(III) dimer complexes.[18] In both examples, the structural trans influence follows the expected order ($NO_2^- > NO_3^-$).

The geometry of the coordinated nitrate group appears normal. The water molecule is hydrogen-bonded to OB3 (2.91 (2) Å) and to NH4 (2.80 (2) Å). The nitrite oxygen atom OD1 forms intramolecular hydrogen bonds to ammine ligands NH4 (2.90 (3) Å) and NH3 (3.09 (2) Å). Both of the nitrite oxygen atoms are not hydrogen-bonded to adjacent molecules, whereas the nitrate oxygen atom OC1(1) participates in three intermolecular hydrogen bonds to two adjacent molecules: OC1(1)···NH3 = 3.09 (3) Å, OC1(1)···NH4 = 3.17 (4) Å, and OC1(1)···NH1 = 3.14 (3) Å. The nitrate oxygen atom OC1(2) also participates in intermolecular hydrogen bonds: OC1(2)···NH1 3.11 (3) Å, OC1(2)···NH3 = 3.20 (3) Å, and OC1(2)···NH4 = 3.25 (4) Å. The geometrical relations of these intermolecular hydrogen bonds are described in Table S4. The nitrate oxygen atom OC3(2) is intermolecularly hydrogen-bonded to NH1 (2.96 (4) Å).

Electrochemical Study. The cyclic voltammogram of **5** in 0.05 M H_2SO_4 is shown in Figure 5. Complex **5** shows an irreversible redox wave in the first cycle at E_{pc} = 0.12 V vs SCE and E_{pa} = 0.70 V; however, in the second and further repetitive cycles, a new quasi-reversible peak appears with increasing intensity at E_{pc} = 0.48 V and E_{pa} = 0.55 V ($E_p = (E_{pc} + E_{pa})/2$ = 0.52 V), and the original irreversible wave gradually decreases. The former irreversible wave corresponds to the reaction **5** + 2e ⇄ **4** + NO_2^- + NO_3^-. The latter quasi-reversible wave corresponds to the reaction **2** + 4e ⇄ 2**4**, since the redox potential is identical with that of the previously reported redox couple, **2** and **4**.[31] Both the two-electron and the four-electron processes seem to be a single wave; however, each of them consists actually of several one-electron processes involving the intermediate oxidation states of the complex, **1** and **3**.[31] The ultraviolet spectrum after bulk reductive electrolysis of complex **5** at −0.2 V in 0.05 M H_2SO_4 shows a shoulder at 240 nm, which is identical with the spectrum previously reported for **4**.[14] The ultraviolet spectrum of **5** and that of an electrochemically reoxidized solution of once reduced **5** in 0.05 M H_2SO_4 are shown in Figure 6. The spectra show that the reoxidized species is not the original **5**; instead, it is tetrameric **2**, which was confirmed by UV spectra (λ_{max}'s for **5** are 294 and 343 nm, while they are 286 and 361 nm for **2**[15] in 0.05 M H_2SO_4). Therefore, on electrochemical reduction, **5** becomes **4**, which is then oxidized to **2** electrochemically. These

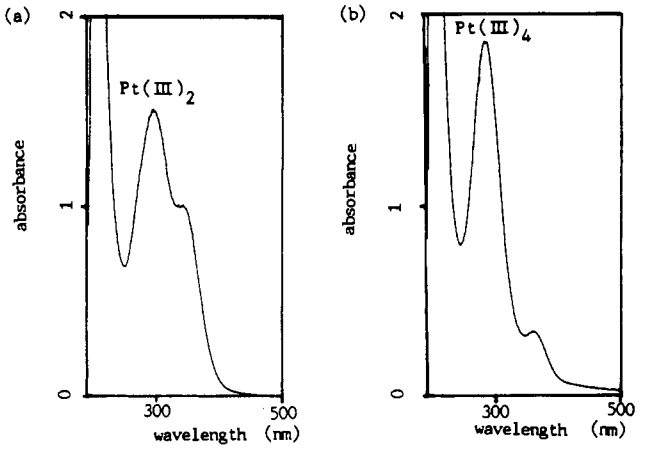

Figure 6. UV–vis spectra of **5** (0.1 mM in 0.05 M H_2SO_4): (a) before electrolysis, (b) after electrolytic reoxidation after reduction at −0.2 V vs SCE.

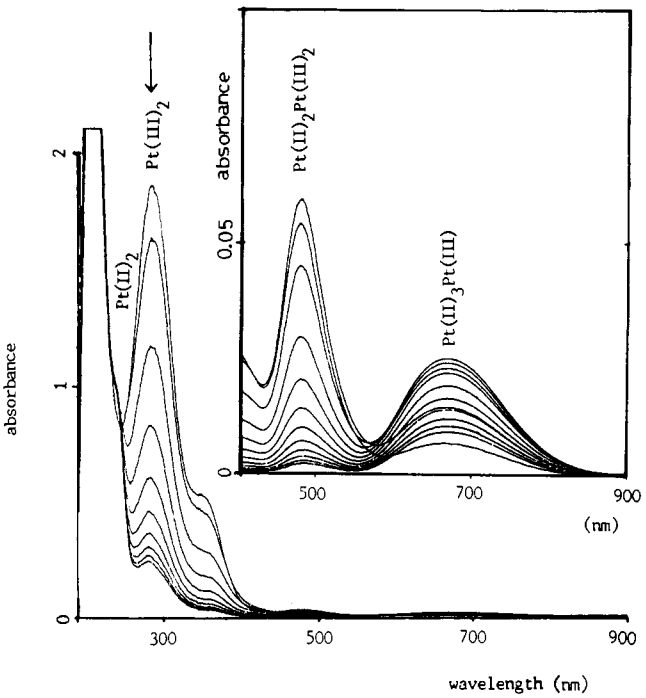

Figure 7. Spectral change of **2** during electrolytic reduction at −0.2 V vs SCE.

redox reactions account for the appearance of the two redox couples in the cyclic voltammogram. Figure 7 shows the spectral change in the UV–vis absorption spectrum during the electrochemical reduction of **5**. It is evident that, as the reduction proceeds, **5** is reduced to **1** and then to **3** and finally to **4** (λ_{max}'s for **1** is 478 and 415 nm, whereas that for **3** is 678 nm[32]). Reoxidation of the electrochemically reduced solution with $Na_2S_2O_8$ also shows absorption bands of **2**.

^{13}C and ^{195}Pt NMR Studies. The ^{13}C CP/MAS spectrum of **5** shown in Figure 2a exhibits α-pyrrolidonate carbon peaks which are in agreement with the crystal structure. The small peaks observed at both sides of the each carbon peak are side bands. Close examination of the spectrum reveals that the peaks C3 and C4 actually consist of two and three peaks, respectively. These splittings reflect the inequivalence of the two bridging α-pyrrolidonate rings, and presumably the inequivalence is due to the two different orientations of the nitrate ligand in the complex. In one of the orientations, shown in Figure 4a, the nitrate ion is almost equally hydrogen-bonded to the two ammine ligands NH1 and NH2, and therefore, the two α-pyrrolidonate rings (plane 1 and

(27) Matsumoto, K. *Bull. Chem. Soc. Jpn.* **1985**, *58*, 651.
(28) Hollis, L. S.; Lippard, S. J. *Inorg. Chem.* **1982**, *21*, 2116.
(29) Hollis, L. S.; Roberts, M. M.; Lippard, S. J. *Inorg. Chem.* **1983**, *22*, 3637.
(30) Hollis, L. S.; Lippard, S. J. *J. Am. Chem. Soc.* **1981**, *103*, 6761.
(31) Matsumoto, K.; Matoba, N. *Inorg. Chim. Acta* **1988**, *142*, 59.
(32) Sakai, K.; Matsumoto, K. *J. Mol. Catal.* **1990**, *62*, 1.

plane 2 in Figure 4a) are equivalent. In the other orientation, shown in Figure 4b, the nitrate ion is relatively strongly hydrogen-bonded to the ammine ligand NH1, and therefore, the two α-pyrrolidonate rings experience trans effects from the ammine ligands to different degrees and would be inequivalent. These differences of the bridging ligands within the molecule give three different environments for the α-pyrrolidonate rings at a relative statistical weight of 2:1:1. The intensities of the three peaks for C4 in Figure 2a are ca. 1:2:1 and reasonably support the inequivalence of the α-pyrrolidonate rings. The peak for C3 splits only into two but this is probably due to the overlapping of the peaks.

In 3.6 M D_2SO_4, each carbon peak does not show any splitting (Figure 2b) except the satellites for C2, which is due to the Pt nucleus ($I = {}^1/_2$, 33.7%). No isomerization between H-H and H-T isomers is observed.

For comparison, ^{13}C and ^{195}Pt NMR spectra of other α-pyrrolidonate-bridged Pt(III) complexes were measured. The ^{13}C spectrum of **2** is basically the same as the spectrum of **5**, which means ^{13}C chemical shift is not considerably affected by whether the complex is tetranuclear or binuclear or by what the axial coordination ligands are. However, the coupling constants $^3J_{C-Pt}$ for the C2 carbon atom are significantly different (see the Results). The ^{195}Pt NMR spectrum of **2** measured at 0 °C shows two peaks at −843 ppm and −316 ppm. These two values correspond to the inner and outer Pt atoms of the tetranuclear complex and are significantly lower than those reported for the analogous α-pyridonate-bridged binuclear Pt(III) complex $[Pt_2(en)_2(C_5H_4NO)_2(NO_2)(NO_3)](NO_3)_2 \cdot 0.5H_2O$ (−1141 and 541 ppm).[18] The solution of **2** is not stable and, if the measurement is carried out overnight at room temperature the peak at −843 ppm diminishes and a new peak appears at 196 ppm. We infer from the chemical shift that this spectral change corresponds to a structural change from the tetranuclear **2** to a binuclear Pt(III) complex similar to **5** although its axial ligands are unknown. However, no convincing evidence supporting this reaction is available at the moment. The reaction is by no means such one as produces a Pt(II) complex via reduction of **2** by water,[15] since the chemical shift is undoubtedly that of a Pt(III) species. We tried to obtain a ^{195}Pt NMR spectrum of **5** in order to compare the spectrum with that of the reaction product of **2**; however, no reliable spectrum was obtained presumably because a very gradual reaction was occurring in the solution.

The ^{13}C NMR spectrum of binuclear Pt(III) complex **6** (Figure 3) suggests that its structure is basically analogous to that of **5** with Me-Im and a sulfate ion as axial ligands. From steric considerations similar to the nitrate and nitrite coordinations in the Pt(III) dimer **5**, it would be reasonable to assume that Me-Im coordinates to the N_2O_2-coordinated Pt atom and a sulfate ion coordinates to the N_4-coordinated Pt atom.

The ^{195}Pt NMR spectrum of **6** shows two peaks at −845 and +205 ppm, which is in agreement with a H-H binuclear Pt(III) structure. The similarity of these chemical shifts to those of the reaction product of **2** (−843 and +196 ppm) suggests that both complexes have a basically similar structure, i.e., a H-H Pt(III) dimer.

Conclusion

The present study demonstrates for the first time the existence of binuclear and tetranuclear α-pyrrolidonate-bridged Pt(III) complexes. Addition of Me-Im to the tetranuclear Pt(III) complex **2** affords the binuclear Pt(III) complex **5**. Oxidation of the mixed-valent tetranuclear complex **1** electrochemically or with $Na_2S_2O_8$ gives the tetranuclear Pt(III) complex **2**, whereas oxidation of **1** by HNO_3 affords the binuclear Pt(III) complex **5**. These facts suggest that axial coordination of significantly strongly coordinating ligands to the tetranuclear complex leads to formation of binuclear Pt(III) complexes. The stabilities of the binuclear Pt(III) complexes versus platinum reduction by water significantly differ depending on the axial ligands.

Acknowledgment. The present study is financially supported by a Grant-in-Aid for Scientific Research on the Priority Area of "Multiplex Organic Systems" (01649008) from the Ministry of Education, Science, and Culture, Japan. Financial support from Asahi Glass Foundation is also gratefully acknowledged. We thank Dr. S. Hayashi of the National Chemical Laboratory for his help in the measurement of CP/MAS NMR spectra.

Registry No. **1**, 80612-40-4; **2**, 100992-71-0; **2a**, 100927-47-7; **5**, 125840-55-3; **5**·H_2O, 125840-56-4; **6**, 136504-59-1; Pt, 7440-06-4; ^{195}Pt, 14191-88-9.

Supplementary Material Available: Details of the X-ray data collection (Table S1), anisotropic temperature factors (Table S2), distances of possible hydrogen bondings (Table S4), and a depiction of the crystal packing (Figure S1) (4 pages); the observed and calculated structure factors (Table S3) (12 pages). Ordering information is given on any current masthead page.

Contribution from the Department of Chemistry, Carnegie Mellon University, 4400 Fifth Avenue, Pittsburgh, Pennsylvania 15213

Design, Synthesis, and Structure of a Macrocyclic Tetraamide That Stabilizes High-Valent Middle and Later Transition Metals

Terrence J. Collins,* Kimberly L. Kostka, Erich S. Uffelman,[1] and Terry L. Weinberger

Received June 28, 1991

High-valent middle and later transition-metal centers tend to oxidatively degrade their ligands. A series of ligand structural features that prevent discovered decomposition routes is presented. The result of the iterative design, synthesis, and testing process described is the macrocyclic tetraamide H_4[**1**]. H_4[**1**] is the parent acid of the macrocyclic tetraamido-*N* ligand $[\eta^4$-**1**$]^{4-}$, which has been shown to stabilize high-valent middle and later transition-metal complexes unavailable in other systems. The features presented provide insights useful to the development of new compounds for homogeneous oxidations and of model compounds for high-valent reactive intermediates in catalytic oxidations in chemistry and biology. The crystal structures of H_4[**1**] and a copper complex of one of its synthetic precursors reveal intramolecular and intermolecular hydrogen bonding patterns that are relevant to recent developments in the ordering effects of hydrogen bonding on solution and solid-state structures. The synthetic value of these ordering effects is discussed.

Introduction

The range of stable high-valent middle and later transition-metal complexes is limited by the small number of suitable ligands. The metal centers in such species usually possess a strong driving force for gaining electrons, and as the nearest source of electrons, the ligand complement is usually vulnerable to one or more of a variety of processes that range from nondestructive polarization in bonding to destructive oxidation events. It is possible to identify the processes and characterize the mechanisms by which a highly

(1) On leave from the California Institute of Technology.

0020-1669/91/1330-4204$02.50/0